catalysts

MDPI

Article

The Catalytic Mechanism of [Bmim]Cl-Transition Metal Catalysts for Hydrochlorination of Acetylene

Hui Shao [1,2], Yingzhou Lu [2], Xin Liang [1,2] and Chunxi Li [1,2,3,*]

[1] State Key Laboratory of Chemical Resource Engineering, Beijing University of Chemical Technology, Beijing 100029, China; shao2020400023@163.com (H.S.); 2009500019@buct.edu.cn (X.L.)
[2] College of Chemical Engineering, Beijing University of Chemical Technology, Beijing 100029, China; 2009500005@buct.edu.cn
[3] Beijing Key Laboratory of Energy Environmental Catalysis, Beijing University of Chemical Technology, Beijing 100029, China
* Correspondence: licx@mail.buct.edu.cn; Tel.: +86-10-64410308

Abstract: Ionic liquids (ILs) are green solvents involved in chemical reaction and separation processes. In this paper, four ILs-based metal catalysts were prepared by dissolving four transition metal chlorides into 1-butyl-3-methylimidazolium chloride ([Bmim]Cl). Their catalytic performance was measured, and the catalytic mechanism was studied via density functional theory (DFT) based on the analysis of the Mayer bonding order, Mulliken charge, molecular electrostatic potential (ESP), electron localization function (ELF), and partial density of states (PDOS). The results show that the catalytic activity follows the order [Bmim]Cl-$RuCl_3$ > [Bmim]Cl-AgCl > [Bmim]Cl-$CuCl_2$ > [Bmim]Cl-CuCl. [Bmim]Cl helps to dissolve and activate HCl, and the metal chlorides can greatly reduce the activation energy of the reaction. This study provides new insights into the catalytic mechanism of IL, transition metals, and their synergistic effect from a microscopic point of view and sheds light on the development of new catalysts for acetylene hydrochlorination.

Keywords: acetylene hydrochlorination; IL-based catalyst; DFT; catalytic mechanism

Citation: Shao, H.; Lu, Y.; Liang, X.; Li, C. The Catalytic Mechanism of [Bmim]Cl-Transition Metal Catalysts for Hydrochlorination of Acetylene. *Catalysts* **2024**, *14*, 93. https://doi.org/10.3390/catal14020093

Academic Editor: Magdalena Zybert

Received: 23 December 2023
Revised: 18 January 2024
Accepted: 22 January 2024
Published: 23 January 2024

1. Introduction

Hydrogen chloride (HCl) is a by-product of many production processes of bulk chemicals, such as methane chloride, chlorinated paraffin, chlorinated polymers, epichlorohydrin, MDI, and TDI. The annual output of HCl in China was about 5 million tons in 2022. Presently, it is reclaimed via water absorption, which not only produces a huge amount of low-quality hydrochloric acids but also devalues its resource uses. In fact, as one of the most widely used top three polymers, over 80% of the vinyl chloride (VCM) is produced through acetylene hydrochlorination due to the resource characteristics of China, which needs a large amount of dry HCl [1]. If the HCl can be directly used for acetylene hydrochlorination, the absorption-reactive desorption and resource utilization HCl byproduct can be realized simultaneously.

As the most commonly used catalyst in the VCM industry, $HgCl_2$ suffers from severe toxicity and volatility and has been being phased out worldwide. Thus, it is very imperative to develop mercury-free alternative catalysts. Hutchings et al. demonstrated the catalytic performance of some precious and transition metal chlorides for acetylene hydrochlorination, e.g., Au(III), Pt(II), Pd(II), Rh(III), Ru(III), Bi(III), and Cu(II) [2–5]. However, the cations are apt to be reduced to metals by the concomitant acetylene and lose their catalysis gradually. To solve this problem, a second metal additive or ionic liquids (ILs) is usually used to improve the stability of the catalyst. The oxidability of the catalytic metallic ions can be regulated via their synergistic interaction with the metallic additives, and the preferential adsorption of HCl in ILs helps to reduce the contact of acetylene with catalytic metals and diminish the reduction of the main catalysts.

Ionic liquids, also known as low-temperature molten salts, can be used as alternative solvents, catalysts, and functional additives for their negligible volatility, good thermochemical stability, high electrical conductivity [6], and easier separation from their mixture with volatile components [7]. These attributes make ILs not only widely used in organic synthesis [8], electrochemistry [9,10], etc., but also as catalysts [11–13] and unique solvents in various separation processes, such as absorption, special rectification, and extraction [14–18]. Many ILs have shown a positive role in the catalytic conversion of acetylene to VCM [19]. Taking [Bmim]Cl as an example, it is an imidazolium-based IL with an N-heterocyclic structure. As a soft Lewis acid, $[Bmim]^+$ may complex with acetylene, a weak, soft acid arising from its well-distributed electrons around the triple bond, reducing the electron cloud density of acetylene and increasing its reactivity. Thus, imidazolium-based ILs show some catalysis for the hydrochlorination of acetylene [20]. ILs not only show high solubility for HCl but also promote its protonation and electrophilic addition reactivity to acetylene. The basicity of N- or P-containing ILs can activate the reactivity of C_2H_2 and HCl to some extent [21]. Cao et al. [22] systematically studied the catalytic effect of some [Bmim]-based ILs in acetylene addition reactions and the influence of the anionic companions. The acetylene conversion rate in [Bmim]Cl is as high as 32%, which is much higher than that in $[Bmim]BF_4$, $[Bmim]PF_6$, or $[Bmim]HSO_4$ ($\leq$3.5%) under same other conditions (10 mL of ILs; reaction at 180 °C; GHSV (C_2H_2) = 40 h^{-1}; V(HCl)/V(C_2H_2) = 1.1~1.2). Therefore, the imidazolium-based chloride catalyst is superior to other anions because it is not only capable of absorbing HCl but also conducive to its protonation to facilitate the reaction.

The solubility of HCl in various imidazolium-based ILs and deep eutectic solvents (DES) has been studied in our group, and the maximum solubility can reach 0.4 $g \cdot g^{-1}$ [23–26]. The as-dissolved HCl can be directly used for the hydrochlorination of acetylene, which not only realizes its in situ utilization but also avoids intensive energy consumption in the desorption process. Generally, the gas–solid phase hydrochlorination is a strong exothermic reaction, which leads to temperature surging and surface carbonization, and compromises the catalysis and lifetime of the catalyst. This phenomenon can be elevated or diminished if the reaction is carried out in liquid, as the reaction heat can be dispatched efficiently to the surrounding liquids under vigorous mixing. Thus, in this paper, we studied the catalysis of some metal chloride-containing ILs catalysts for the hydrochlorination of acetylene in a batch reactor, to which acetylene and HCl in definite mole ratio were purged and dissolved simultaneously, and then reacted at a higher temperature for a period of time. This process can simulate the absorption of HCl and its in situ reactive desorption at high temperatures, which is of great significance for the effective utilization of HCl.

2. Results and Discussion

2.1. Catalytic Performance of the IL-Based Catalysts

In this paper, the catalytic performance of three ILs, i.e., [Emim]Cl, [Bmim]Cl, and [Hmim]Cl, on hydrochlorination of acetylene were first investigated. The abbreviation of the ILs, catalysts, and the terminologies used is listed in Text S1 for clarity. The structure of the ILs was verified by ^{1}H NMR and ^{13}C NMR (see Text S2), and the GC-MS of acetylene hydrochlorination is presented in Figure S1. As shown in Figure S2, the neat ILs show definite catalytic performance with 20~22% acetylene conversion and 95–96% VCM selectivity, which is consistent with the reported results for the bubbling reaction [22]. On the contrary, the conversion of acetylene in the absence of ILs is only 0.5% at the same experimental condition. In the reaction systems, there exists a π-π interaction between C_2H_2 and the imidazolium cations, as confirmed by the quantum chemical calculation and molecular dynamics simulation [27], and the alkyl-substituent is of little influence on the interaction. Thus, [Bmim]Cl was chosen in the following studies for its liquidity at room temperature and easy availability. To further enhance its catalytic performance, it is necessary to add some transition metal chloride (CuCl, $CuCl_2$, AgCl, or $RuCl_3$) that has intrinsic catalysis on the reaction. As such, the metal chloride can be dissolved and complexed with [Bmim]Cl, forming an ILs-based metal chloride complex ([Bmim]Cl-MCl_n, M = Cu^+, Cu^{2+}, Ag^+, Ru^{3+},

denoted as B1, B2, B3, and B4, respectively). Their catalytic performance at varying ratios of [Bmim]Cl to MCl_n was studied, and the results are presented in Figure 1a–d. The thermal stability of these catalysts was assessed by TG analysis, and the results are shown in Figure S3. The slight mass loss before 100 °C is ascribed to water vaporization of the ILs, and their mass loss was all within 2.3% at 160 °C, showing relatively high thermal stability. The metal chloride amount added to [Bmim]Cl and detected by ICP is listed in Table 1.

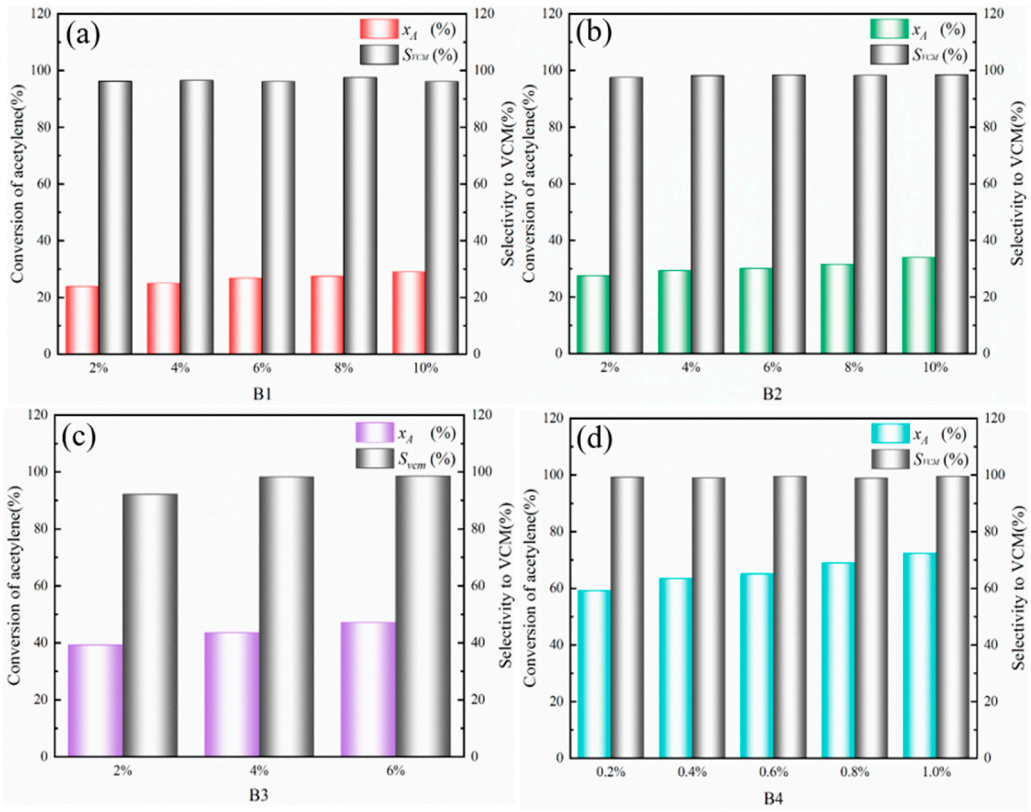

Figure 1. Acetylene conversion and vinyl chloride selectivity according to different catalysts at the fixed reaction condition (160 °C, n_{HCl}/n_{C2H2} = 1~1.2, 1 h). (**a**) B1: [Bmim]Cl-CuCl; (**b**) B2: [Bmim]Cl-$CuCl_2$; (**c**) B3: [Bmim]Cl-AgCl; (**d**) B4: [Bmim]Cl-$RuCl_3$.

Table 1. Metal chloride amount added to [Bmim]Cl and detected by ICP.

Catalyst	Content of Metal Chlorides
[Bmim]Cl-CuCl (10%)	9.93%
[Bmim]Cl-$CuCl_2$ (10%)	9.88%
[Bmim]Cl-AgCl (6%)	5.93%
[Bmim]Cl-$RuCl_3$ (1%)	0.98%

As shown in Figure 1a–d, the acetylene conversion in all catalysts is increased slightly with the increasing content of metal chlorides, and the catalytic activity follows the order B4 >> B3 > B2 > B1. Specifically, the acetylene conversion rate slightly increased from 23.9% to 29.1% for catalyst B1, as the CuCl content increased from 2% to 10%, along with the VCM selectivity of 96%. Similarly, the conversion rate of acetylene increased from 27.6% to 34.0% for catalyst B2, as the $CuCl_2$ content increased from 2% to 10% with the same VCM selectivity of 96%. In contrast, catalyst B3 shows better catalytic performance, and the acetylene conversion rate increased from 39.2% to 47.2% as the AgCl content increased from 2% to 6%. B4 shows the best catalytic performance; the acetylene conversion rate can reach 59.3% with only 0.2% $RuCl_3$ addition and further increased to 72.3% at 1.0%

$RuCl_3$, and the VCM selectivity is about 98.5%. Thus, [Bmim]Cl-$RuCl_3$ can be deemed as a promising catalyst for the hydrochlorination of acetylene.

2.2. Structural and Electronic Properties of the IL-Based Catalysts

To give better insights into the catalytic performance difference of the catalysts, molecular surface electrostatic potential (ESP) analysis was performed on the catalysts and their corresponding components. As shown in Figure 2, there is an ESP minimum (-61.64 kcal·mol^{-1}) near Cl^- on [Bmim]Cl. All the metal chlorides show ESP maximum near the metal ions, following the order of CuCl (+85.9 kcal·mol^{-1}) > AgCl (+71.35 kcal·mol^{-1}) > $RuCl_3$ (+38.93 kcal·mol^{-1}) > $CuCl_2$ (+29.61 kcal·mol^{-1}), which are greater than the ESP minimum around Cl ion. This suggests that the metal chloride can easily approach and complex with the Cl ion of [Bmim]Cl. In addition, the ESP maxima of the HCl molecule (+43.1 kcal·mol^{-1}) is greater than the minimum (-10.26 kcal·mol^{-1}); thus, the HCl molecule is also prone to approaching Cl^- of [Bmim]Cl. The results indicate that [Bmim]Cl can anchor both metal ions and HCl molecules. The optimized configurations of the IL-based catalysts are shown in Figure S4.

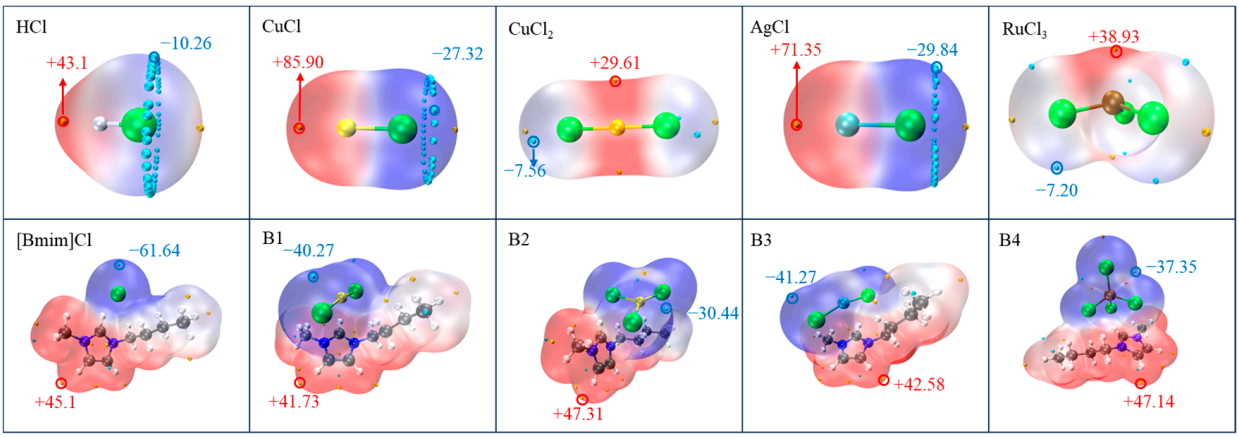

Figure 2. Electrostatic potential diagrams of different substances. (The transition from red to blue indicates a decrease in electrostatic potential).

Atomic charge, also known as point charge located at the center of an atom, can be used to study the state of atoms in various chemical environments and molecular properties [28], predict reaction sites, etc. [29,30]. In this paper, we studied the atomic charge of the catalysts using Mulliken charge analysis. The Mulliken charges of neat [Bmim]Cl and B1–B4 were 0.749 *e*, 0.371 *e*, 0.383 *e*, 0.471 *e*, and 0.385 *e*, respectively. Table S1 records the electron transfer between catalysts and the reactants or products once they are in contact. Due to the strong interaction between HCl and IL-based catalysts, the number of electrons gained by HCl from the catalyst follows the order [Bmim]Cl (0.322 *e*) > B3 (0.129 *e*) > B1 (0.105 *e*) > B2 (0.07 *e*) > B4 (0.059 *e*), mainly arising from the electron transfer between Cl^- to the proton of HCl, forming hydrogen-bonding $Cl^- \rightarrow$HCl. Meanwhile, C_2H_2 and C_2H_3Cl transfer their electrons to the catalysts B1-B4, except for [Bmim]Cl, due to their electron richness and electron-donating attributes.

To further understand the reactivity or stability of the chemicals involved in the reaction system, we analyzed their highest occupied molecular orbital (HOMO) and the lowest unoccupied molecular orbital (LUMO), as shown in Figures 3 and S5. The HOMO/LUMO values and energy gap for both reactants and catalysts are shown in Table S2. It is noted that the energy gap of LUMO(HCl)−HOMO(IL) is smaller than that of LUMO(IL)−HOMO(HCl), while the energy gap of LUMO(C_2H_2)−HOMO(IL) is higher than that of LUMO(IL)−HOMO(C_2H_2). This suggests that the electrons of the IL-based catalyst tend to pass to HCl rather than acetylene. In Figure 3, the HOMO orbitals of the catalyst are distributed on Cl^- or the complex anions, which further justify the electrons

transfer from the IL-based catalysts to HCl. The energy gap of LUMO (HCl)−HOMO(IL) is smaller than that of LUMO(C_2H_2)−HOMO(IL), which suggests the preferential adsorption of HCl versus acetylene on the catalysts.

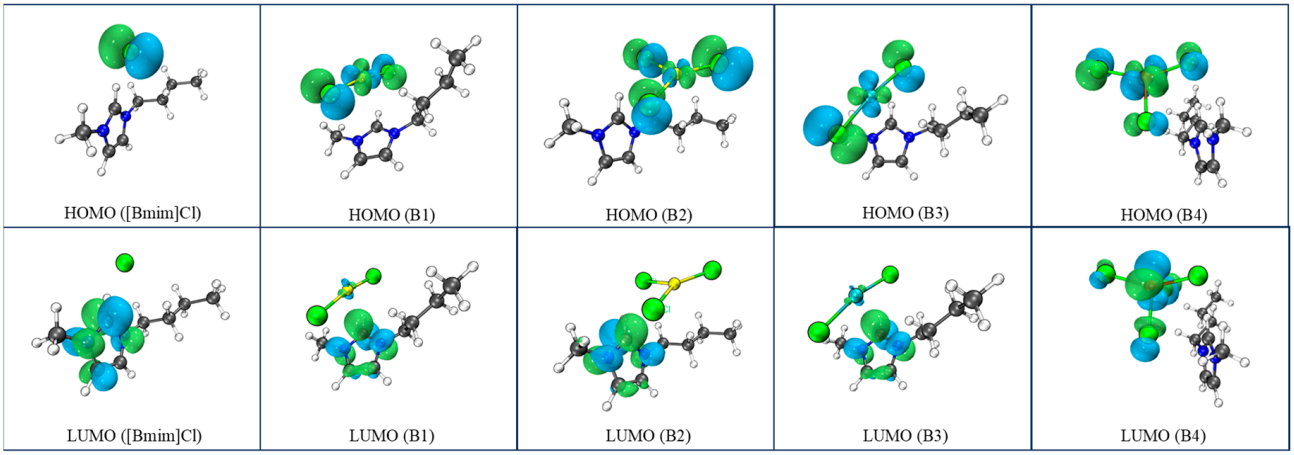

Figure 3. HOMO and LUMO orbitals of different IL-based catalysts. (White = H, black = C, blue = N, green = Cl, yellow = Cu, cyan = Ag, brown = Ru. Blue and green bubbles represent the HOMO/LUMO orbital distribution).

2.3. Interaction between Catalysts and Reactants and Product

The interaction modes and strength of ILs-based catalysts with reactants and products directly affect their catalytic activity [19] and the catalytic mechanism. The most stable intermolecular interaction configuration is shown in Figure 4. In the neat [Bmim]Cl, Cl^- is prone to complex with the 2-H and the alpha-H of the imidazolium ring via weak H-bonding [22]. Upon absorption, the HCl molecule is also complexed with Cl^- of the ILs-based catalysts, with their H-bonding length varying from 1.633 to 2.203 Å (see first column of Figure 4). As a result, the bond length of HCl is stretched to 0.229, 0.041, 0.027, 0.064, and 0.034 Å, respectively, for [Bmim]Cl and B1–B4 catalysts. In addition, the pair-wise interaction energies of [Bmim]Cl and B1–B4 with HCl were −19.55 kcal·mol^{-1}, −11.17 kcal·mol^{-1}, −9.15 kcal·mol^{-1}, −11.89 kcal·mol^{-1}, and −10.78 kcal·mol^{-1}, respectively. The interaction energy follows the order [Bmim]Cl > B3 > B1 > B4 > B2. Thus, [Bmim]Cl-HCl has the strongest interaction, which results in a higher solubility and dissociation of HCl molecules. The Mayer bond order of the HCl molecule, when paired with different catalysts, varies from 0.539 to 0.885, which is much lower than that of the free HCl molecule of 0.994 (Table S3). Further, the variation of the bond order of HCl and its interaction energy with different catalysts follows the same order. Thus, the covalent bond of the HCl molecule is weakened and activated by the coexisted IL catalysts [31].

On the contrary, the bond length of acetylene experiences little change (1.207~1.209 Å) when paired with the catalysts. The interaction energy of acetylene with the catalysts varied in the range of −4.08~−7.37 kcal·mol^{-1}, and that of C_2H_3Cl with the catalysts varied in the range of −5.49~−8.94 kcal·mol^{-1}, which are lower than those of HCl. This further confirms the preferential interaction of the IL-based catalysts with HCl rather than C_2H_2, which is consistent with frontier orbital theory analysis.

The preferential capture of HCl by ILs helps to inhibit C_2H_2 polymerization and reduce the coking on the catalytically active centers, which in turn improves their catalytic stability [32]. As seen from the Gibbs free energies in Table 2, the adsorption of VCM on all catalysts is nonspontaneous ($\Delta G > 0$); that is to say, VCM can be easily released from the catalysts, preventing its polymerized deposition therein.

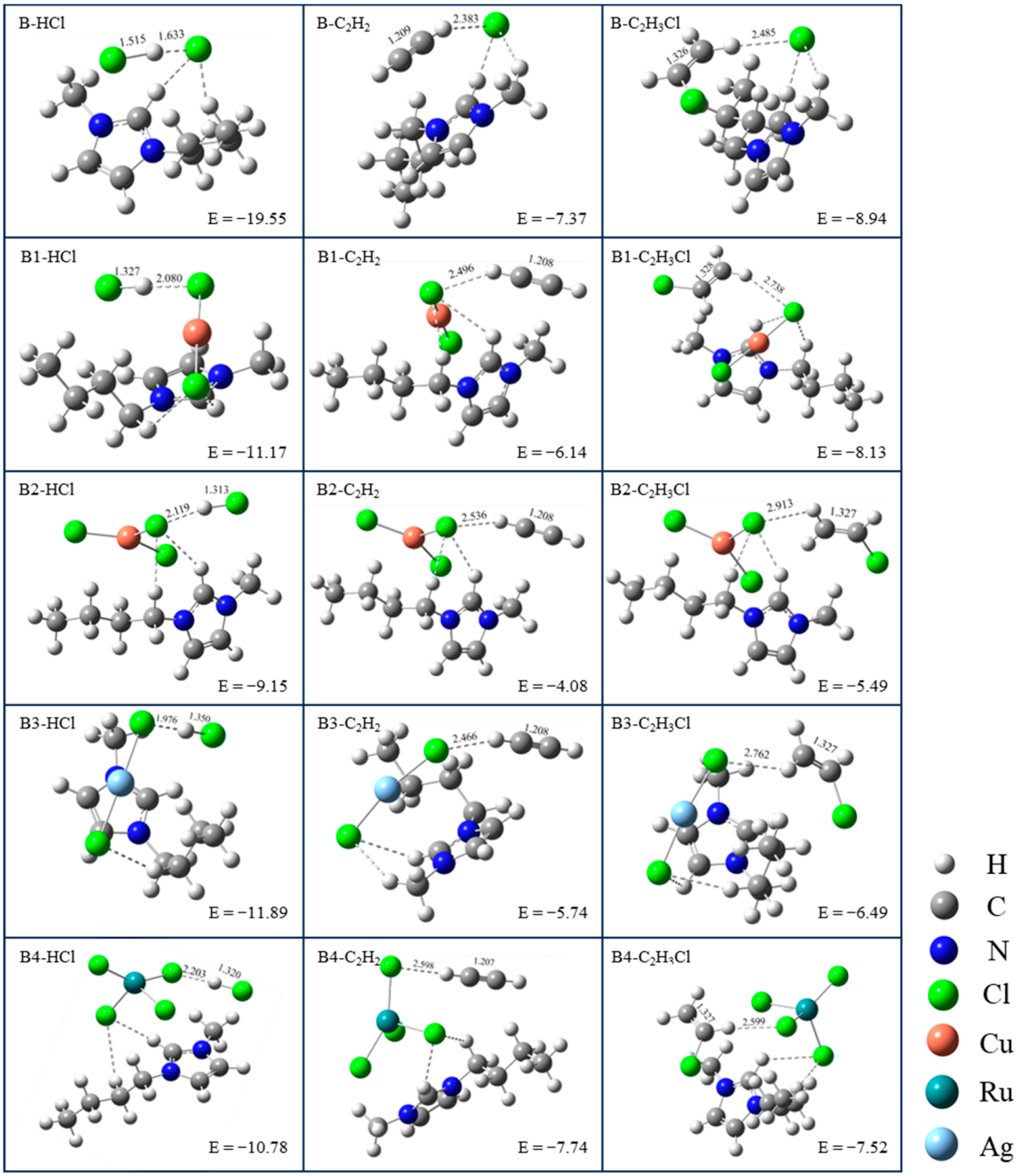

Figure 4. Configuration and interaction energy *E* of HCl, C_2H_2, and C_2H_3Cl with different catalysts.

Table 2. Gibbs free energy for the interaction of HCl, C_2H_2, and C_2H_3Cl with different catalysts.

ΔG/kcal·mol^{-1}	BM	B1	B2	B3	B4
HCl	−10.4	−2.87	−0.2	−2.64	−1.05
C_2H_2	0.53	1.73	2.68	2.61	1.52
C_2H_3Cl	1.28	0.11	2.02	3.82	1.28

The interaction between IL-based catalysts and the chemicals involved can be reflected in the change of the IR peaks. The IR spectra of all catalysts in the presence of HCl, C_2H_2, and VCM were simulated using Gaussian software under the 6-31(d,p) basis set and the scaling factor of 1.0008 [33]. The experimental and simulated IR spectrum of [Bmim]Cl is compared in Figure S6. The broad peak centered around 3440 cm^{-1} is mainly attributed to

the O-H of water impurity and the weak stretching vibration of C-H in the imidazolium ring with a DFT simulated value of 3297 cm^{-1}. The peaks 3000~3300 cm^{-1} correspond to the stretching and wobbling vibration of the C-H bonds of methyl and butyl in [Bmim]Cl. The simulated peaks of 1589 and 1204 cm^{-1} are the deformation vibrations of the imidazolium ring, which is slightly larger than the experimental ones (1571.7 and 1170 cm^{-1}). The simulated peaks of 1302 cm^{-1} and 735 cm^{-1} denote the wobble vibrations and out-of-plane wobble vibrations of C-H of imidazolium, respectively, which are slightly lower than the experimental values (1337 and 755 cm^{-1}). The simulated peak at 2625 cm^{-1} for C-H stretching vibration at the 2-position of imidazolium is not observed experimentally. Overall, the simulated IR spectra of [Bmim]Cl are virtually consistent with the experimental one; thus, the IR spectra variation in the presence of HCl, C_2H_2, and VCM will be analyzed based on the simulated IR spectra hereafter.

As shown in Figures 5 and S7 and Table S4, the C-H stretching vibration of the imidazolium at 2-position shifts significantly from 2625 to 3188~3269 cm^{-1} in the presence of different metal salts. However, the dissolved C_2H_3Cl, C_2H_2, and HCl molecules have a marginal influence on the shift of this peak. This implied a strong interaction between the C-H bond of imidazolium at the 2-position and metal chloride, which is consistent with the ESP analysis in Section 2.2.

The C-H stretching vibration (3180~3300 cm^{-1}), the shear vibration peak (1676~1684 cm^{-1}), and the in-plane and out-of-plane bending vibration (932~1052 cm^{-1}) peaks of VCM show a relatively small shift in all catalysts. Similarly, the C-H asymmetric stretching vibration (V^{as}, 3200~3400 cm^{-1}), the symmetric stretching vibration (V^{s}, 2050 cm^{-1}), and the in-plane and out-of-plane bending vibration (β and γ, 814~896 cm^{-1}) peaks of C_2H_2 are shifted slightly in all catalysts. This justified the relatively weak interaction between different catalysts and C_2H_2 or VCM.

In contrast, the IR spectra of HCl in [Bmim]Cl are quite different from those in catalysts B1-B4. Specifically, the stretching vibration peak of HCl in [Bmim]Cl (301 cm^{-1}) is shifted to much higher wavenumbers in catalyst B1–B4 (2170~2600 cm^{-1}). This may be ascribed to the complexation between metal chloride (Lewis acid) and Cl^-, which reduced the H-bonding ($Cl^- \rightarrow$HCl) interaction and enhanced the bond strength and wavenumbers of the HCl molecule. However, the out-of-plane(ω) and in-plane(ρ) rocking vibration peaks (901 cm^{-1} and 785 cm^{-1}) of HCl in [Bmim]Cl are shifted to lower wavenumbers (500~651 cm^{-1} and 445~629 cm^{-1}) in B1–B4 catalysts, which may be attributed to the stronger H-bonding interaction between HCl and [Bmim]Cl in the absence of metal chlorides. The purple box regions in Figure 5 show the characteristic vibrational peak of the M-Cl bond in catalysts B1–B4.

2.4. Reaction Mechanisms

To better understand the reaction mechanism of acetylene hydrochlorination, a DFT simulation was conducted based on the TS method and Eley–Rideal (ER) reaction mechanism. First, the transition state structure of different IL-based catalysts was predicted for the hydrochlorination of acetylene. Second, the intrinsic reaction coordinates(IRC) scanning was performed using the energy saddle point of the transition state, evolved to the intermediate(INT) state and adsorption(Ads) state, respectively, via forward and backward scans, and then verified the catalysis. The energy changes and structural configurations during the catalytic reaction process are shown in Figures 6 and 7 and Table S5. The ER-catalyzed mechanism has two key steps, i.e., generation of the VCM intermediate (C_2H_2Cl*) and its protonation [31,34–36]. Each step has a corresponding transition state (TS) and intermediate product, and the specific conformational details of the co-adsorption, transition state, and intermediate product are shown in Figure S8.

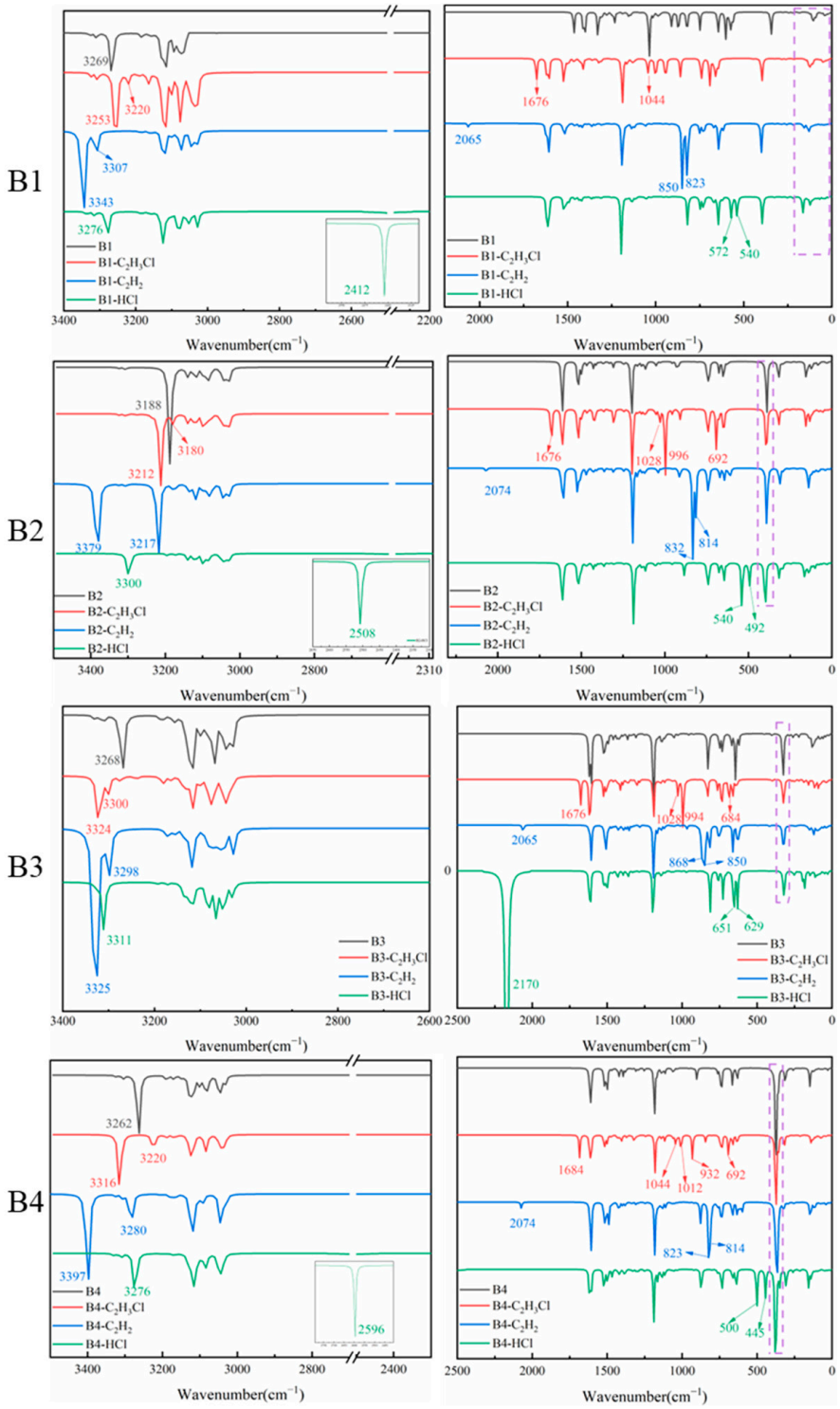

Figure 5. Simulated IR spectra of catalysts B1–B4 in presence of C_2H_2, HCl, and VCM.

According to the above analysis, IL-based catalysts tend to preferentially adsorb HCl, and the HCl approaches the Cl^- of the catalysts through H-bonding, forming HCl-ILs. Then, C_2H_2 is trapped by the HCl-ILs, forming a co-adsorption configuration (Ads). In the resulting co-adsorption structure of [Bmim]Cl and B1–B4, the H-bonding length between H(1) of HCl and Cl^-(2) is 1.767 Å, 2.054 Å, 2.06 Å, 1.973 Å, and 2.166 Å, respectively. Acetylene molecules are adsorbed on the metal sites (Cu/Ag/Ru) of the catalysts or on Cl^- of [Bmim]Cl. In the co-adsorption configuration of B1–B4, a "hammer-like" stable structure is formed between acetylene and metal ions of the catalysts, and the interatomic

distance of M-C(1) varies in the range of 2.022~2.708 Å, depending on the size of the metal ions. The interatomic distance between C(2)-H and Cl(2) in [Bmim]Cl is 2.445 Å. In this section, all the Δ*G* of the co-adsorption process in [Bmim]Cl and catalyst B1–B4 is negative, and their values follow the order B4(−9.49 kcal·mol^{-1}) < [Bmim]Cl (−7.87 kcal·mol^{-1}) < B1(−2.91 kcal·mol^{-1}) < B2 (−2.11 kcal·mol^{-1}) < B3 (−1.11 kcal·mol^{-1}), indicating the stable existence of these adsorption configurations.

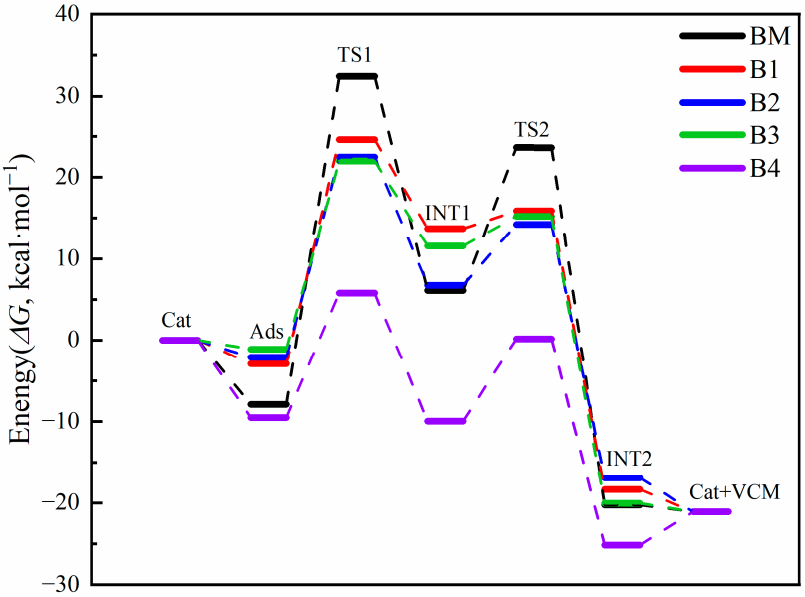

Figure 6. Energy change of catalytic reaction process.

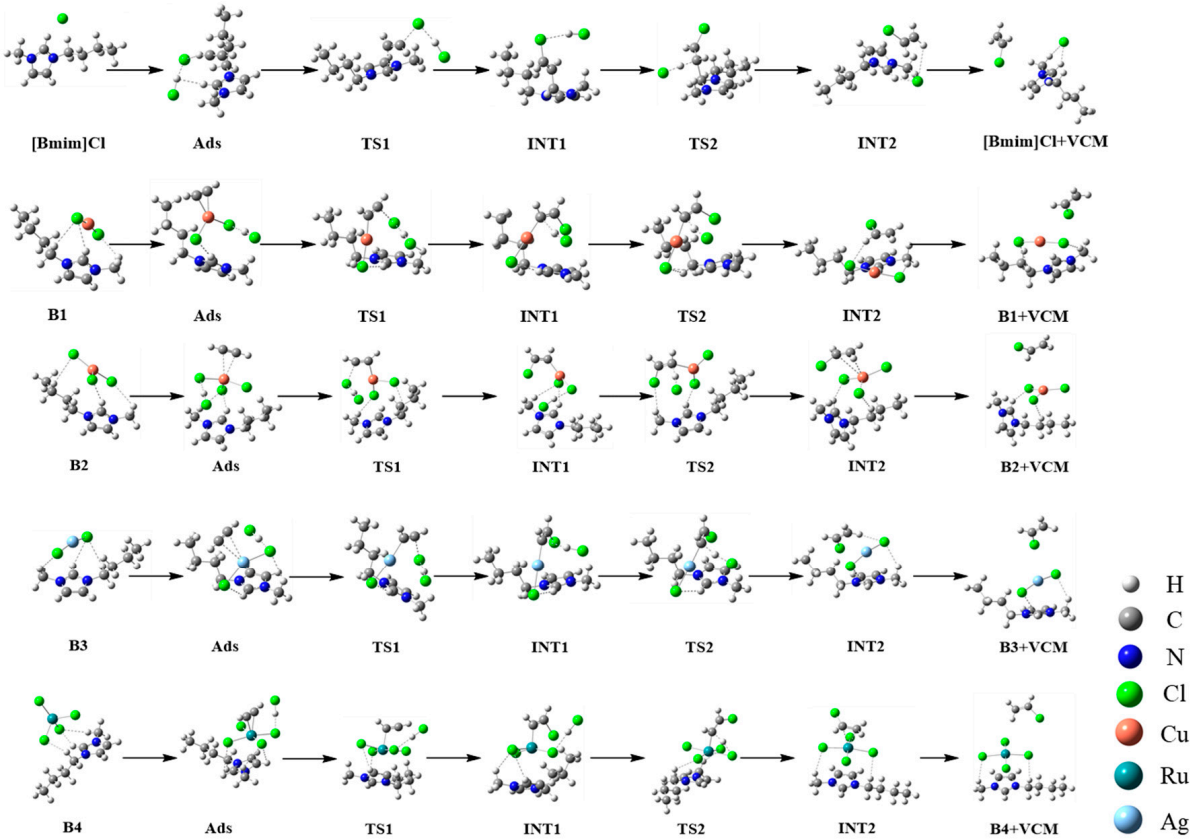

Figure 7. Conformational changes of the catalytic reaction process.

The formation of the transition state TS1 is the key step in the acetylene hydrochlorination reaction [34]. In this process, the linear structure of C_2H_2 is disrupted, and the C≡C bond length is increased from (1.210~1.236) Å to (1.257–1.260) Å, depending on the type of the catalyst. The bond angle of C(1)≡C(2)-H is decreased from 180° to (137~151)°, and the acetylene is activated significantly. In this process, the M^{n+}-Cl(2) bond of the metal chlorides is stretched and broken, with their bond length prolonged from (2.305, 2.250, 2.458, and 2.397 Å) to (3.441, 2.609, 3.486, and 2.476)Å, respectively for catalysts B1–B4. The C(1) of acetylene and metal ion forms a new C-M bond, with its bond length being 1.927 Å, 2.006 Å, 2.136 Å, and 2.085 Å, respectively. At the same time, Cl(2) in the catalyst is trapped by C(2) of the acetylene molecule, forming the intermediate (C_2H_2Cl*). The active energy of this step with different catalysts follows the order B4 (15.27 kcal·mol^{-1}) < B3 (23.11 kcal·mol^{-1}) < B2 (24.56 kcal·mol^{-1}) < B1 (27.51 kcal·mol^{-1}). This indicates that $RuCl_3$ has better catalytic activity than AgCl, $CuCl_2$, and CuCl, which is consistent with the previous experimental observation. The reaction energy barrier in pure [Bmim]Cl is 40.31 kcal·mol^{-1}, which is significantly higher than that in IL-based metal chloride catalysts. Thus, for an acetylene hydrochlorination reaction, the catalytic activity mainly depends on the metal ions of the catalysts in specified ILs [37].

Accompanying the formation of intermediate INT1, the energy drop is 26.26, 10.91, 15.71, 10.43, and 15.73 kcal·mol^{-1}, respectively, in [Bmim]Cl and B1–B4, due to the reconstruction of the chemical bonds, i.e., the formation of C(2)-Cl(2) and the conversion of C(1)≡C(2) of acetylene to C(1)=C(2). Subsequently, the HCl molecule is adsorbed by the electron-rich intermediate C_2H_2Cl*, and its bond is stretched from (1.296~1.329) Å to (1.528~1.597) Å. The H(1)-Cl(1) bond breaks as H(1) attacks the C=C of C_2H_2Cl*, and Cl(1) is attracted by the IL-based catalyst, forming the intermediate VCM*, also known as the transition state TS2. At this state, the distance of the C(1)-H(1) of VCM* is 1.437 Å, 1.424 Å,1.419 Å, 1.454 Å, and 1.431 Å, respectively, in catalysts [Bmim]Cl and B1~B4. The reaction active energy ΔG in [Bmim]Cl and B1–B4 is 17.57, 2.18, 7.5, 3.63, and 10.12 kcal·mol^{-1}, respectively. From TS2 to INT2, H(1) of HCl combines with the C atom of C_2H_2Cl* to form the co-adsorption product INT2, accompanying a large energy release of 43.89, 34.23, 31.14, 35.25, and 25.31 kcal·mol^{-1}, respectively, for [Bmim]Cl and B1–B4 catalysts. Overall, TS1 is the most energy-demanding step in the whole process and is the controlling step of the reaction [38,39]. Generally speaking, the addition of appropriate metal chloride to [Bmim]Cl can slightly enhance the adsorption of acetylene and HCl but significantly reduce the activation energy of the key reaction step, especially $RuCl_3$, making the activation energy lower than that of pure [Bmim]Cl by 25.04 kcal·mol^{-1}. Thus, $RuCl_3$ is an excellent catalyst for the hydrochlorination of acetylene.

2.5. Electron Density and Orbital Bonding Analysis

In the chemical reaction process, the electron transfer between reactants is usually mediated by the catalyst, and the intermolecular interaction between reactant and catalyst pairs is crucial. Thus, the Electron Localization Function (ELF) is used to analyze the electron distribution of different reactant-catalyst pairs, and the Partial Density of States (PDOS) is used to analyze the bond changes in different catalytic stages.

In the ELF diagram, the color from cold to warm represents an increased electron density in the region. As shown in Figure 8, there exists a higher LOL (localized orbital locator) value between Cl^- of [Bmim]Cl and H of HCl (or C_2H_2), i.e., a certain degree of electron overlaps there. In other words, Cl^- of [Bmim]Cl is prone to transferring its electron to the proton of HCl or C_2H_2, resulting in a significant increase in electron density between them. However, for the pairwise interaction between catalyst(B1–B4) and HCl (or C_2H_2), the LOL value between HCl and Cl^- of the catalyst is higher than that between acetylene and Cl^-, along with a closer interatomic distance, suggesting a stronger interaction with HCl. This is because the electron cloud density of Cl^- in [Bmim]Cl is delocalized into its

metal chloride complex in B1–B4, which greatly decreases the negative charge of each Cl atom and electrostatic interaction with HCl and acetylene.

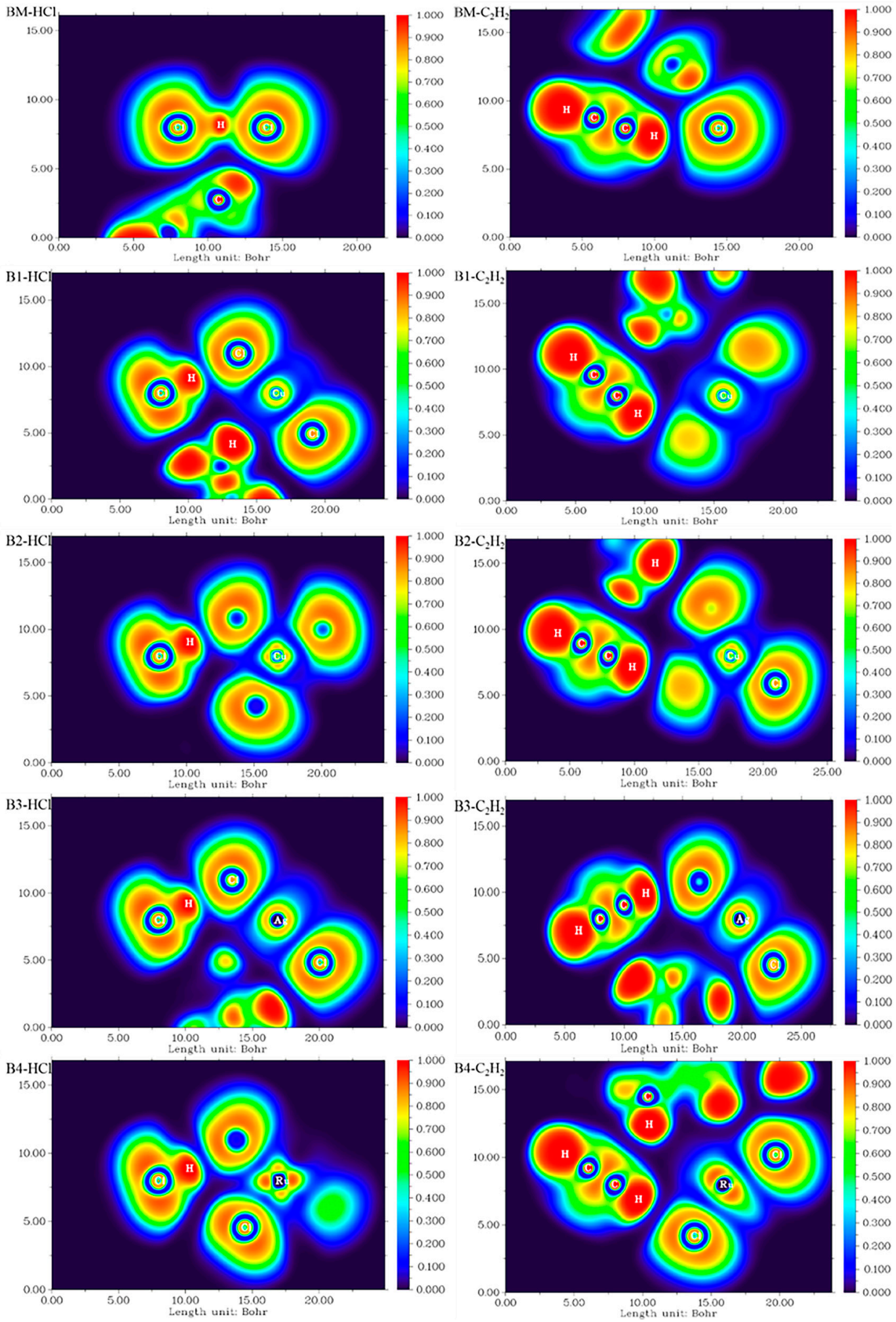

Figure 8. ELF plots for different reactant–catalyst pairs.

In order to investigate the bonding between two spatially adjacent atoms, we analyzed the PDOS at different catalytic reaction stages in different catalysts. For illustration, the PDOS map of the catalytic reaction process in [Bmim]Cl is presented in Figure 9 and analyzed in detail, and the PDOS maps for other catalysts are shown in Figures S9–S12.

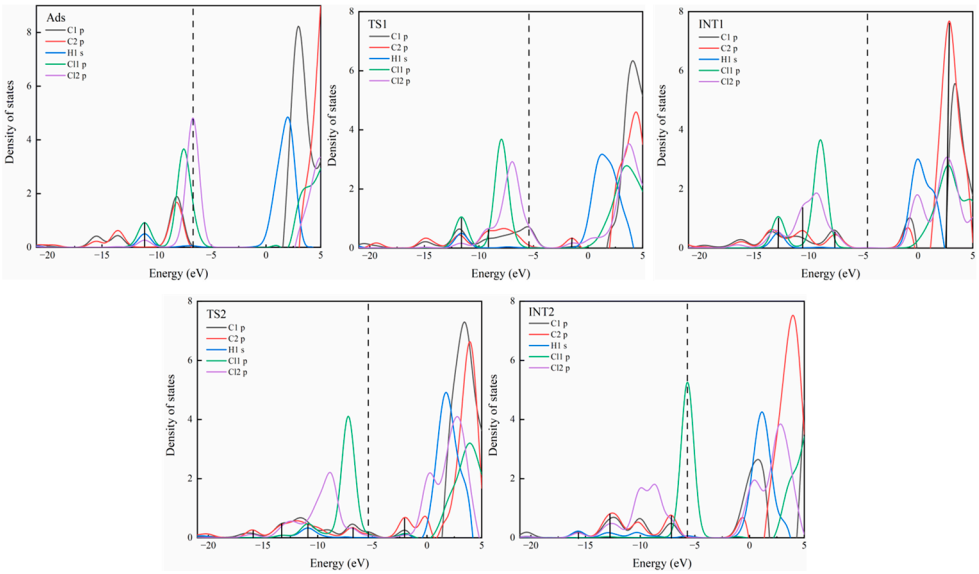

Figure 9. PDOS of the catalytic reaction process in [Bmim]Cl. Vertical black lines represent areas with peak overlapping. The dashed black line represents the HOMO value.

As seen in Figure 9, in the co-adsorption structure Ads, the s-orbital of H(1) in HCl and the p-orbital of Cl(2) in [Bmim]Cl are hybridized and overlapped at ca. −11 eV, which is in agreement with the ELF analysis. In [Bmim]Cl-TS1, the p-orbital profiles of C(1) and C(2) are no longer identical, especially in the range of −5~−10 eV, and the p-orbital of Cl(2) has hybridized with C(2) at ca. −11.5 eV. This suggests that the C(1)≡C(2) bond of C_2H_2 is broken and begins to move closer to the Cl(2) of [Bmim]Cl. In the intermediate product [Bmim]Cl-INT1, the curve changes of the p-orbitals of C(1) and C(2) are converging again at ca. −7.5 eV and −10.5 eV, and the p-orbital peaks are completely wrapped by the p-orbital peaks of Cl(2) in the range of −5~−12.5 eV. This indicates that vinyl chloride intermediate ($C_2H_2Cl^*$) is completely generated, and the C(1)≡C(2) triple bond is replaced by a C(1)=C(2) double bond.

In [Bmim]Cl-TS2, the s-orbital of H(1) is completely covered by the p-orbital of C(1) at -6 and -11 eV. This suggests that the H(1)-Cl(1) bond of HCl is completely broken, the proton H(1) gradually approaches C(1) in the intermediate. The hybridization between H(1) and C(1) is enhanced, while the overlap area or hybridization between the s-orbital of H(1) and p-orbital of Cl(1) of HCl becomes smaller, but still partially hybridized.

The PDOS of the catalytic reaction process in catalysts(B1-B4) is only slightly different from those in [Bmim]Cl, mainly due to the different adsorption structures of acetylene. In the catalysts(B1-B4), acetylene is adsorbed around the metal ions, leading to hybridization between C(1) and C(2) of acetylene and the metal ions M^{n+}. During the transition from Ads to TS1, the bond between M^{n+} and C(1) of acetylene remains, and C(2) is attacked by Cl(2), leading to the breakage of the C(2)-M bond. After the formation of the intermediate INT1, the C(1)-M bond disappears due to the attack of C(1) by H(1) of HCl, and the metal ion M captures the Cl(1) of HCl, forming a new M-Cl bond.

3. Materials and Methods

3.1. Materials

Analytical-grade chemicals were purchased from Shanghai Macklin Biochemical Technology Co., Ltd., including 1-ethyl-3-methylimidazolium chloride ([Emim]Cl, ≥97.0 wt%),

1-butyl-3-methylimidazolium chloride ([Bmim]Cl, ≥97 wt%), 1-hexyl-3-methylimidazolium chloride ([Hmim]Cl, ≥97 wt%), cuprous chloride (CuCl, ≥98 wt%), copper chloride ($CuCl_2$, ≥98 wt%), silver chloride (AgCl, ≥97 wt%), and ruthenium chloride trihydrate ($RuCl_3 \cdot 3H_2O$, ≥37 wt%), and used as received without further purification. Nitrogen (N_2, 99.999%) was purchased from Beijing Haipu Gas Co., Ltd., and hydrogen chloride (HCl, 99.9%) was purchased from Beijing Guante Gas Co., Ltd.

3.2. Catalyst Preparation

Taking [Bmim]Cl-AgCl (2 wt%) as an example, 2.5 g of [Bmim]Cl and 0.05 g of AgCl were added to a 100 mL glass vial and stirred magnetically at 80 °C for 2 h until a transparent liquid was formed. The as-prepared liquid catalyst was dried in a vacuum oven at 60 °C for 12 h to remove trace amount of water. Other metal-chloride-based IL catalysts were prepared similarly.

3.3. Catalyst Tests

Scheme 1 shows the reaction setup for acetylene hydrochlorination. First, 2.5 g of catalyst was added into the stainless steel reactor, and then the air inside was evacuated using a vacuum pump to prevent its interference with the reaction. To the reactor, 0.1~0.15 MPa acetylene and 0.2~0.3 MPa hydrogen chloride were purged successively with a specific mole ratio at 1~1.2 [40] through the high-pressure gas cylinder. Then, the reactor was placed into a thermostatic electric heating jacket and stirred at 160 °C for 1 h. After reaction, the reactor was taken out and cooled to room temperature naturally.

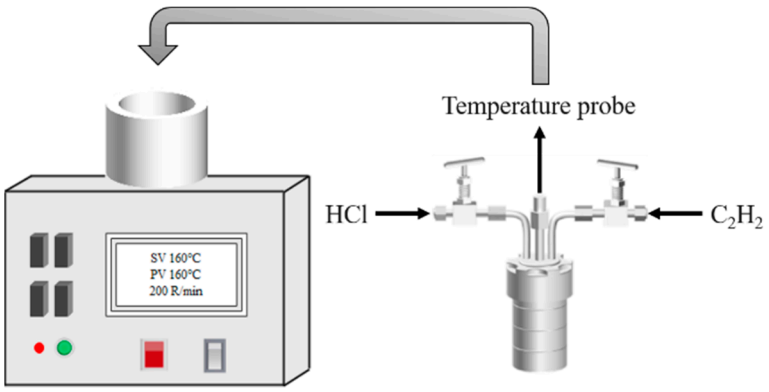

Scheme 1. The reaction setup for the catalytic hydrochlorination of acetylene.

The gas product was sampled with a gas bag, and its composition was detected by a gas chromatograph (GC 2010, Shimadzu) with Agilent HP-Al/KCl column (length of 50 m, film thickness of 15 μm, inner diameter of 0.53 mm, upper temperature limit of 200 °C), FID detector, and split ratio of 16.8. The gasification chamber and detector temperature were both 250 °C. The temperature of the chromatographic column was maintained at 100 °C. The carrier gas was nitrogen with flow rate of 5.08 mL·min^{-1}. The conversion of acetylene (x_A) and selectivity to VCM (S_v) were calculated by the following equations:

$$x_A = \frac{\varphi_{A0} - \varphi_A}{\varphi_{A0}} \quad (1)$$

$$S_v = \frac{\varphi_v}{1 - \varphi_v} \times 100\% \quad (2)$$

where φ_{A0}, φ_A, and φ_v represent the volume fraction of acetylene in the feed and product gases and volume fraction of VCM in the product, respectively.

3.4. Characterization

The thermal stability of the catalyst was evaluated by TGA (TGA 550, TA Instruments, Newcastle, DE, USA). The experiments were carried out under a nitrogen atmosphere at a flow rate of 20 mL·min^{-1}, and the temperature was increased from 30 °C to 800 °C at 10 K·min^{-1}.

The catalysts were characterized by FTIR (Nicolet iS20, Thermo fisher Scientific, Waltham, MA, USA). The liquid samples were tested in ATR mode within the wave number range of 600~4000 cm^{-1}.

^{1}H NMR and ^{13}C NMR (AVANCE III HD 400, Bruker, Billerica, MA, USA) of three ILs were tested to ensure their structure. The ILs were dissolved in deuterated DMSO and tested under a magnetic field of 400M/500M. The metal content in the IL-based catalysts was analyzed by ICP-OES (Agilent 5800, Agilent, CA, USA). The reaction products were determined by GC-MS (GCMS-QP2020, Shimadzu, Kyoto, Japan).

3.5. Density Functional Calculation

In this paper, unconstrained geometry optimization and DFT calculations were performed using Gaussian software and the B3LYP method (Becke's three-parameter hybrid generalization B3 combined with Lee–Yang–Parr (LYP)) correlation generalization for all atoms [41]. In the structural optimization, frequency calculation, and transition state determination, 6-31G (d,p) basis set was used for H, C, N, O, and Cl elements, and a pseudopotential basis set SDD was used for Ru, Cu, and Ag elements. For the calculation of single-point energy, the 6-311++G (2d,p) basis set was used for H, C, N, O, and Cl, and the pseudopotential basis set def2-tzvp was used for Ru and Ag.

Frequency calculation was performed to determine all steady-state points as transition states with one imaginary frequency or minima without imaginary frequency. IRC was calculated for all transition states to confirm that the structures indeed connect the two associated minima. All calculations were performed using the Gaussian 09 software package. Charge distributions, Mayer bond order, Mulliken charge, ESP, ELF, and PDOS were analyzed using the Multiwfn analysis program [42–44].

The energy (E) reported in this paper is the sum of the electron energy and the zero-point energy correction, and the Gibbs energy (G) is the sum of the electron energy and the thermal free energy correction. To analyze the interaction of reactants (HCl, C_2H_2), product (vinyl chloride), and IL, the interaction energy (E) is defined in Equation (3) [45]:

$$E = E_{adsorption} - E_{free\ molecule} - E_{IL} \quad (3)$$

where $E_{adsorption}$ is the total energy of C_3H_2Cl, C_2H_2, or HCl paired with the IL-based catalyst; $E_{free\ molecule}$ is the energy of C_3H_2Cl, C_2H_2, or HCl; and E_{IL} is the energy of each IL-based catalyst. ΔG is calculated in the same way.

4. Conclusions

Four IL-based complex catalysts were synthesized by dissolving specific amounts of CuCl, $CuCl_2$, AgCl, and $RuCl_3$, respectively, in [Bmim]Cl. [Bmim]Cl-$RuCl_3$ has the best catalytic performance, showing a 72.3% acetylene conversion rate at 1% wt $RuCl_3$ usage and experimental conditions of 160 °C, n_{HCl}/n_{C2H2} = 1~1.2, 1 h. [Bmim]Cl can form H-bonding with the dissolved HCl, prolong the bond length of HCl, and enhance its reactivity. The electron transfers from the HOMO of [Bmim]Cl to LUMO of HCl via H-bonding interaction, promoting nucleophilic attack of HCl to C_2H_2. The reaction activation energy can be reduced and the conversion rate of acetylene enhanced greatly by adding transition metal chlorides. The activation energy is decreased by 25.04 kcal·mol^{-1} in [Bmim]Cl-$RuCl_3$ compared to that in [Bmim]Cl. The transition metal ions and ILs can synergistically catalyze the hydrochlorination of acetylene.

Supplementary Materials: The following Supporting information can be downloaded at: https://www.mdpi.com/article/10.3390/catal14020093/s1, Text S1: List of abbreviations in the manuscript; Text S2: ^{1}H NMR and ^{13}C NMR analysis of ionic liquids; Figure S1. Gas chromatograms (a) and mass Spectra (b-d) of the gases after the reaction; Figure S2: Acetylene conversion and vinyl chloride Selectivity by ILs at the fixed reaction condition; Figure S3: TG curves of different IL-based catalysts; Figure S4: Structure of five IL-based catalysts; Figure S5: HOMO/LUMO orbitals of HCl and C_2H_2; Figure S6: Comparison between the IR experiment Spectrum and the DFT Simulation Spectrum of [Bmim]Cl; Figure S7: Simulated IR Spectra of [Bmim]Cl in presence of C_2H_2, HCl, and VCM; Figure S8: Configuration details during catalytic process; Figure S9: PDOS of the catalytic reaction process on B1; Figure S10: PDOS of the catalytic reaction process on B2; Figure S11: PDOS of the catalytic reaction process on B3; Figure S12: PDOS of the catalytic reaction process on B4; Table S1: Mulliken charge changes in adsorption configuration; Table S2: HOMO and LUMO values and energy gaps of different Substances; Table S3: Mayer bond order of HCl on different catalysts; Table S4: Peak positions of IR Spectra after catalysts absorbing C_2H_3Cl, C_2H_2, and HCl (cm^{-1}); Table S5: Data for energy changes in ER mechanism for acetylene hydrochlorination ($kcal \cdot mol^{-1}$).

Author Contributions: Conceptualization, H.S. and C.L.; Data curation, H.S.; Formal analysis, H.S. and C.L.; Funding acquisition, C.L.; Investigation, H.S. and C.L.; Methodology, H.S. and C.L.; Project administration, C.L.; Resources, C.L.; Software, H.S.; Supervision, C.L.; Validation, H.S.; Visualization, H.S.; Writing—original draft, H.S.; Writing—review and editing, Y.L., X.L. and C.L. All authors have read and agreed to the published version of the manuscript.

Funding: The authors are grateful for the financial support from the National Natural Science Foundation of China (No. 21978006).

Data Availability Statement: Most of the data that support the findings of this study are available in the article and supplementary material. Any additional data not found in the above locations can be made available from the corresponding author upon reasonable request.

Acknowledgments: The quantitative calculation data in this paper are supported by the high-performance computing platform BUCT.

Conflicts of Interest: The authors declare no conflicts of interest.

References

1. Zhang, J.; Liu, N.; Li, W.; Dai, B. Progress on cleaner production of vinyl chloride monomers over non-mercury catalysts. *Front. Chem. Sci. Eng.* **2011**, *5*, 514–520. [CrossRef]
2. Hutchings, G.J. Vapor phase hydrochlorination of acetylene: Correlation of catalytic activity of supported metal chloride catalysts. *J. Catal.* **1985**, *96*, 292–295. [CrossRef]
3. Nkosi, B.; Coville, N.J.; Hutchings, G.J. Vapour phase hydrochlorination of acetylene with group VIII and IB metal chloride catalysts. *Appl. Catal.* **1988**, *43*, 33–39. [CrossRef]
4. Hutchings, G.J.; Grady, D.T. Effect of drying conditions on carbon supported mercuric chloride catalysts. *Appl. Catal.* **1985**, *16*, 411–415. [CrossRef]
5. Nkosi, B.; Coville, N.J.; Hutchings, G.J.; Adams, M.D.; Friedl, J.; Wagner, F.E. Hydrochlorination of acetylene using gold catalysts: A study of catalyst deactivation. *J. Catal.* **1991**, *128*, 366–377. [CrossRef]
6. Hallett, J.P.; Welton, T. Room-Temperature Ionic Liquids: Solvents for Synthesis and Catalysis. 2. *Chem. Rev.* **2011**, *111*, 3508–3576. [CrossRef] [PubMed]
7. Vekariya, R.L. A review of ionic liquids: Applications towards catalytic organic transformations. *J. Mol. Liq.* **2017**, *227*, 44–60. [CrossRef]
8. Toshiyuki, I.; Eri, A.; Kazutoshi, K.; Shohei, S. Lipase-Catalyzed Enantioselective Acylation in the Ionic Liquid Solvent System: Reaction of Enzyme Anchored to the Solvent. *Chem. Lett.* **2001**, *30*, 262–263. [CrossRef]
9. Tang, Y.; Liu, X.; McMahan, J.; Kumar, A.; Khan, A.; Sevilla, M.; Zeng, X. Adsorption and Electrochemistry of Carbon Monoxide at the Ionic Liquid–Pt Interface. *J. Phys. Chem. B* **2019**, *123*, 4726–4734. [CrossRef]
10. Cabral, D.M.; Howlett, P.C.; MacFarlane, D.R. Electrochemistry of the tris(2,2′-bipyridine) complex of iron(II) in ionic liquids and aprotic molecular solvents. *Electrochim. Acta* **2016**, *220*, 347–353. [CrossRef]
11. Martini, M.B.; Fernández, J.L.; Adam, C.G. Insights on the catalytic behaviour of sulfonic acid-functionalized ionic liquids (ILs) in transesterification reactions—Voltammetric characterization of sulfonic task-specific ILs with bisulfate anions. *Phys. Chem. Chem. Phys.* **2021**, *23*, 2731–2741. [CrossRef] [PubMed]
12. Kore, R.; Berton, P.; Kelley, S.P.; Aduri, P.; Katti, S.S.; Rogers, R.D. Group IIIA Halometallate Ionic Liquids: Speciation and Applications in Catalysis. *ACS Catal.* **2017**, *7*, 7014–7028. [CrossRef]

13. Song, Z.; Huang, W.; Zhou, Y.; Tian, Z.-Q.; Li, Z.-M.; Tao, D.-J. Thermally regulated molybdate-based ionic liquids toward molecular oxygen activation for one-pot oxidative cascade catalysis. *Green Chem.* **2020**, *22*, 103–109. [CrossRef]
14. Taylor, S.F.R.; McClung, M.; McReynolds, C.; Daly, H.; Greer, A.J.; Jacquemin, J.; Hardacre, C. Understanding the Competitive Gas Absorption of CO_2 and SO_2 in Superbase Ionic Liquids. *Ind. Eng. Chem. Res.* **2018**, *57*, 17033–17042. [CrossRef]
15. Ávila, J.; Lozano-Martín, D.; Simões Santos, M.; Zhang, Y.; Li, H.; Pádua, A.; Atkin, R.; Costa Gomes, M. Effect of ion structure on the physicochemical properties and gas absorption of surface active ionic liquids. *Phys. Chem. Chem. Phys.* **2023**, *25*, 6808–6816. [CrossRef]
16. Sosa, J.E.; Ribeiro, R.P.P.L.; Castro, P.J.; Mota, J.P.B.; Araújo, J.M.M.; Pereiro, A.B. Absorption of Fluorinated Greenhouse Gases Using Fluorinated Ionic Liquids. *Ind. Eng. Chem. Res.* **2019**, *58*, 20769–20778. [CrossRef]
17. Gui, C.; Li, G.; Zhu, R.; Liu, Q.; Lei, Z. Ionic Liquids for Capturing 1,2-Dimethoxyethane (DMET) in VOCs: Experiment and Mechanism Exploration. *Ind. Eng. Chem. Res.* **2022**, *61*, 2257–2267. [CrossRef]
18. Zhu, R.; Huang, S.; Gui, C.; Li, G.; Lei, Z. Capturing low-carbon alcohols from CO_2 gas with ionic liquids. *Chem. Eng. Sci.* **2022**, *258*, 117745. [CrossRef]
19. Nian, Y.; Zhang, J.; Li, X.; Wang, Y.; Li, W.; Kolubah, P.D.; Han, Y. Molecular design of ionic liquids as novel non-metal catalysts for the acetylene hydrochlorination reaction. *Phys. Chem. Chem. Phys.* **2019**, *21*, 7635–7644. [CrossRef]
20. Wang, B.; Lai, H.; Yue, Y.; Sheng, G.; Deng, Y.; He, H.; Guo, L.; Zhao, J.; Li, X. Zeolite Supported Ionic Liquid Catalysts for the Hydrochlorination of Acetylene. *Catalysts* **2018**, *8*, 351. [CrossRef]
21. Hu, J.; Yang, Q.; Yang, L.; Zhang, Z.; Su, B.; Bao, Z.; Ren, Q.; Xing, H.; Dai, S. Confining Noble Metal (Pd, Au, Pt) Nanoparticles in Surfactant Ionic Liquids: Active Non-Mercury Catalysts for Hydrochlorination of Acetylene. *ACS Catal.* **2015**, *5*, 6724–6731. [CrossRef]
22. Zhou, X.; Xu, S.; Liu, Y.; Cao, S. Mechanistic study on metal-free acetylene hydrochlorination catalyzed by imidazolium-based ionic liquids. *Mol. Catal.* **2018**, *461*, 73–79. [CrossRef]
23. He, R.-H.; Long, B.-W.; Lu, Y.-Z.; Meng, H.; Li, C.-X. Solubility of Hydrogen Chloride in Three 1-Alkyl-3-methylimidazolium Chloride Ionic Liquids in the Pressure Range (0 to 100) kPa and Temperature Range (298.15 to 363.15) K. *J. Chem. Eng. Data* **2012**, *57*, 2936–2941. [CrossRef]
24. Zhu, J.; Shao, H.; Feng, L.; Lu, Y.; Meng, H.; Li, C. Absorptive separation of HCl gas by choline chloride-based deep eutectic solvents. *J. Mol. Liq.* **2021**, *341*, 116928. [CrossRef]
25. Feng, L.; Meng, H.; Lu, Y.; Li, C. Efficient and reversible absorption of HCl gas by ChCl-based deep eutectic solvents-Insights into the absorption behavior and mechanism. *Sep. Purif. Technol.* **2022**, *281*, 119994. [CrossRef]
26. Shao, H.; Zhu, J.; Feng, L.; Liang, X.; Lu, Y.; Meng, H.; Li, C. Solubility Behavior and the Mechanism of HCl Gas in Four [EMIM]Cl-Based Deep Eutectic Solvents. *J. Chem. Eng. Data* **2022**, *67*, 3097–3107. [CrossRef]
27. Zhao, X.; Xing, H.; Yang, Q.; Li, R.; Su, B.; Bao, Z.; Yang, Y.; Ren, Q. Differential Solubility of Ethylene and Acetylene in Room-Temperature Ionic Liquids: A Theoretical Study. *J. Phys. Chem. B* **2012**, *116*, 3944–3953. [CrossRef]
28. Qian, B.H.; Wei-Xing, M.A.; Lu-De, L.U.; Yang, X.J.; Wang, X. Synthesis, Characterization, Crystal Structure and Quantum Chemistry Calculation of an Arenedisulfonate Bridged Zn(II) Coordination Polymer. *Acta Phys. Chim. Sin.* **2010**, *26*, 610–616. [CrossRef]
29. Zheng, W.R.; Xu, J.L.; Xiong, R. Density Functional Theory Study on N–O Bond Dissociation Enthalpies. *Acta Phys. Chim. Sin.* **2010**, *26*, 2535–2542. [CrossRef]
30. Shen, T.; Du, F.P.; Liu, T.; Yao, G.W.; Wu, Z.; Fang, M.M.; Xu, X.J.; Lu, H.Z. Molecular Simulation of the Interaction between Imidazole Glycerol Phosphate Dehydrase and Nitrogen-Containing Heterocyclic Phosphate Inhibitors. *Acta Phys. Chim. Sin.* **2011**, *27*, 1831–1838. [CrossRef]
31. Li, Y.; Wang, F.; Hu, J.; Sun, M.; Wang, J.; Zhang, X. A study on the rules of ligands in highly efficient Ru–amide/AC catalysts for acetylene hydrochlorination. *Catal. Sci. Technol.* **2021**, *11*, 7347–7358. [CrossRef]
32. Zhao, J.; Gu, S.; Xu, X.; Zhang, T.; Yu, Y.; Di, X.; Ni, J.; Pan, Z.; Li, X. Supported ionic-liquid-phase-stabilized Au(iii) catalyst for acetylene hydrochlorination. *Catal. Sci. Technol.* **2016**, *6*, 3263–3270. [CrossRef]
33. Kesharwani, M.K.; Brauer, B.; Martin, J.M.L. Frequency and Zero-Point Vibrational Energy Scale Factors for Double-Hybrid Density Functionals (and Other Selected Methods): Can Anharmonic Force Fields Be Avoided? *J. Phys. Chem. A* **2015**, *119*, 1701–1714. [CrossRef] [PubMed]
34. Ren, Y.; Wu, B.; Wang, F.; Li, H.; Lv, G.; Sun, M.; Zhang, X. Chlorocuprate(i) ionic liquid as an efficient and stable Cu-based catalyst for hydrochlorination of acetylene. *Catal. Sci. Technol.* **2019**, *9*, 2868–2878. [CrossRef]
35. Zhang, T.; Wang, B.; Nian, Y.; Liu, M.; Jia, Y.; Zhang, J.; Han, Y. Excess Copper Chloride Induces Active Sites over Cu-Ligand Catalysts for Acetylene Hydrochlorination. *ACS Catal.* **2023**, *13*, 8307–8316. [CrossRef]
36. Wang, B.; Zhang, T.; Liu, Y.; Li, W.; Zhang, H.; Zhang, J. Phosphine-oxide organic ligand improved Cu-based catalyst for acetylene hydrochlorination. *Appl. Catal. A Gen.* **2022**, *630*, 118461. [CrossRef]
37. Li, X.; Nian, Y.; Shang, S.; Zhang, H.; Zhang, J.; Han, Y.; Li, W. Novel nonmetal catalyst of supported tetraphenylphosphonium bromide for acetylene hydrochlorination. *Catal. Sci. Technol.* **2019**, *9*, 188–198. [CrossRef]
38. Li, H.; Wu, B.; Wang, J.; Wang, F.; Zhang, X.; Wang, G.; Li, H. Efficient and stable Ru(III)-choline chloride catalyst system with low Ru content for non-mercury acetylene hydrochlorination. *Chin. J. Catal.* **2018**, *39*, 1770–1781. [CrossRef]

39. Zhang, Y.; Li, S.; Qiao, X.; Guan, Q.; Li, W. Efficient and stable N-heterocyclic ketone–Cu complex catalysts for acetylene hydrochlorination: The promotion effect of ligands revealed from DFT calculations. *Phys. Chem. Chem. Phys.* **2023**, *25*, 25581–25593. [CrossRef]
40. Gu, J.; Gao, Y.; Zhang, J.; Li, W.; Dong, Y.; Han, Y. Hydrochlorination of Acetylene Catalyzed by an Activated Carbon-Supported Ammonium Hexachlororuthenate Complex. *Catalysts* **2017**, *7*, 17. [CrossRef]
41. Li, J.; Zhang, H.; Li, L.; Cai, M.; Li, Y.; Xie, D.; Zhang, J. Synergistically Catalytic Hydrochlorination of Acetylene over the Highly Dispersed Ru Active Species Embedded in P-Containing Ionic Liquids. *ACS Sustain. Chem. Eng.* **2020**, *8*, 10173–10184. [CrossRef]
42. Lu, T.; Chen, F. Multiwfn: A multifunctional wavefunction analyzer. *J. Comput. Chem.* **2012**, *33*, 580–592. [CrossRef] [PubMed]
43. Liu, Z.; Lu, T.; Chen, Q. An sp-hybridized all-carboatomic ring, cyclo[18]carbon: Electronic structure, electronic spectrum, and optical nonlinearity. *Carbon* **2020**, *165*, 461–467. [CrossRef]
44. Zhang, J.; Lu, T. Efficient evaluation of electrostatic potential with computerized optimized code. *Phys. Chem. Chem. Phys.* **2021**, *23*, 20323–20328. [CrossRef]
45. Zhou, X.; Zhu, M.; Kang, L. Single-Atom X/g-C_3N_4 (X = Au_1, Pd_1, and Ru_1) Catalysts for Acetylene Hydrochlorination: A Density Functional Theory Study. *Catalysts* **2019**, *9*, 808. [CrossRef]